

# RELATIVISTIC COULOMB EXCITATION: FROM RISING TO PreSPEC\*

HANS-JÜRGEN WOLLERSHEIM

GSI Helmholtzzentrum für Schwerionenforschung  
Planckstrasse 1, 64291 Darmstadt, Germany

*(Received February 15, 2011)*

The new PreSPEC project will be presented with an advanced particle (LYCCA) and  $\gamma$ -ray (AGATA) detection system as compared to the RISING set-up. This contribution focuses on planned Coulomb excitation experiments at relativistic energies. Characteristic parameters are presented, followed by the experimental conditions for experiments at 100 A MeV and feasibility studies for future measurements.

DOI:10.5506/APhysPolB.42.705

PACS numbers: 29.25.Rm, 29.30.-h, 25.70.De, 25.70.-z

## 1. Introduction

In 2003 the Rare ISotopes INvestigation at GSI project [1] started which combines the former EUROBALL Ge-Cluster detectors, the MINIBALL Ge detectors, BaF<sub>2</sub>-HECTOR detectors, and the FRagment Separator (FRS) at GSI for high-resolution in-beam  $\gamma$ -ray spectroscopy measurements with radioactive beams. These secondary beams produced at relativistic energies were used for Coulomb excitation or secondary fragmentation experiments in order to explore the nuclear structure of the projectiles or projectile like nuclei by measuring de-excitation photons. In those experiments the FRS provided selection, identification and tracking of the incoming particle on the secondary target. Gold targets of 400 mg/cm<sup>2</sup> thickness were bombarded at the final focus for Coulomb excitation experiments. The reaction products were selected using the calorimeter telescope array CATE [2] consisting of an array of  $3 \times 3$  Si-CsI(Tl)  $\Delta E - E$  telescopes. The energy loss in the Si detectors provided unambiguous  $Z$  identification after the secondary target.

---

\* Presented at the Zakopane Conference on Nuclear Physics “Extremes of the Nuclear Landscape”, August 30–September 5, 2010, Zakopane, Poland.

The total energy measurement of the fragments was, however, insufficient to completely distinguish masses. Position sensitivity of the Si detectors enabled scattering angle determination.

The  $\gamma$ -rays emitted by the reaction products were measured in the Coulomb excitation experiments with 15 Cluster Ge detectors, containing 7 crystals, positioned in three rings at extreme forward angles of  $16^\circ$ ,  $33^\circ$  and  $36^\circ$ . The full energy efficiency of this arrangement amounts to 2.9% for 1.3 MeV  $\gamma$ -rays emitted at  $v/c = 0.5$ . For some experiments up to 8 six-fold segmented MINIBALL triple Ge detectors were arranged in two rings with central angles of  $45^\circ$  and  $85^\circ$  relative to the beam line at forward angles. The position sensitivity of the MINIBALL detectors allowed them to be placed at a close target distance of 250 mm, while the Cluster detectors sat at larger distances of 700 mm in order to obtain an energy resolution of  $\sim 1.2\%$ .

Relativistic Coulomb excitation was used in several experiments in order to extract absolute  $B(E2)$  values of the first excited state in unstable nuclei. In the isotopes  $^{56}\text{Cr}$  and  $^{58}\text{Cr}$  the results confirm the sub-shell closure at  $N = 32$  [3]. In the  $^{108}\text{Sn}$  isotope the obtained  $B(E2)$  value shows an unexpected enhancement as compared to neutron-rich tin isotopes [4]. Besides the observation of the first excited  $2^+$  state, relativistic Coulomb excitation of  $^{136}\text{Nd}$  at RISING allowed to populate also the second excited  $2^+$  state and to deduce three  $B(E2)$  values of this triaxial nucleus [5]. The obtained  $\gamma$ -ray spectrum clearly demonstrates the high quality which can be achieved by optimal background reduction and Doppler correction in the analysis. In a Coulomb excitation experiment at 600 A MeV evidence was found for the presence of a pygmy resonance in the neutron-rich  $^{68}\text{Ni}$  nucleus which is energetically located below the GDR [6].

## 2. PreSPEC

To fully exploit the exotic beams, lasting problems in detection efficiency have to be solved. They result from limited radioactive beam intensity, discrimination of reaction products due to rather thick secondary target, and high  $\gamma$ -ray and particle background. The finite thickness of the secondary target seriously limited the envisaged mass resolution of CATE. A time-of-flight measurement must be added into the system being a compromise between flight path, *i.e.*, solid angle coverage, and the time resolution of the detectors used ( $\Delta t \sim 100$  ps). LYCCA (Lund–York–Cologne CALorimeter) deals with ions up to  $A \sim 200$  at energies up to 100 A MeV. In its final version it is a core device for the HISPEC-DESPEC [7] program, which is part of the NUSTAR [8] Collaboration within FAIR [9]. The main objective of LYCCA is tracking as well as mass and charge determination of the outgoing particle from the secondary target. In the PreSPEC campaign all specific components for particle identification (LYCCA-0) and high-resolution  $\gamma$ -ray

spectroscopy (AGATA [10] demonstrator array) will be incorporated in order to prepare the HISPEC-DESPEC program. In 2010 PreSPEC will start with the implementation of LYCCA-0 which will comprise four central LYCCA modules with polycrystalline CVD diamond detectors and eight surrounding LYCCA-CATE (CsI) modules. LYCCA-0 is located about 3.1 m behind the secondary target and covers angles of  $\Delta\theta \sim \pm 3.0^\circ$  which are the relevant ones in relativistic Coulomb excitation measurements at 100 A MeV.

For the second stage of the PreSPEC fast beam campaign, between 2011–2013, the AGATA demonstrator array will be the main  $\gamma$ -ray detector to perform in-beam  $\gamma$ -ray spectroscopy experiments at the FRS. The  $\gamma$ -ray tracking system involves measuring the position and energy of every  $\gamma$ -ray interaction in a detector so that path and sequential energy-loss of a single  $\gamma$ -ray can be deduced using the Compton-scattering formula. Since the first interaction in the  $\gamma$ -ray detector is important for the Doppler correction, AGATA will represent a dramatic advantage in  $\gamma$ -ray detection. The AGATA demonstrator array is an arrangement of ten triple clusters and five double clusters which has a standard target-detector distance of 23.5 cm for spherical symmetry. Since  $\gamma$ -ray tracking is performed, one obtains the best performance of the array by a shift from the geometrical center. The calculations show that the photopeak efficiency of the  $1\pi$  array is 18% for  $v/c = 0.5$ , with an energy resolution of 0.3%. This represents an increase of a factor of 6 in efficiency compared with RISING in singles and even higher for coincidence spectroscopy.

This contribution focuses on planned Coulomb excitation experiments with the PreSPEC project at the SIS/FRS fragmentation facility. Some characteristic parameters are presented, followed by the conditions for relativistic Coulomb excitation and feasibility studies for future experiments.

### 3. Characteristic parameters of Coulomb excitation

Although quantum-mechanical calculations are performed for heavy-ion scattering, the understanding of reactions between heavy ions is greatly facilitated by applying semi-classical concepts to these processes. An approximate condition for classical behavior is given by the *Sommerfeld parameter*

$$\eta = \frac{a}{\lambda} \quad \text{with} \quad a = \frac{Z_1 Z_2 e^2}{m_0 c^2 \beta^2} = \frac{1.44 \times Z_1 Z_2 (A_1 + A_2)}{931.5 \times A_1 A_2 \times \beta^2} \quad [\text{fm}] \quad (1)$$

which must be large compared to unity:  $\eta \gg 1$ . Here  $a$  is half the distance of closest approach in a head-on collision (neglecting the nuclear field) and  $\lambda$  is the reduced wavelength at infinite ion separation. In Eq. (1)  $Z_1$ ,  $A_1$  and  $Z_2$ ,  $A_2$  denote charge and mass numbers of projectile and target nucleus, respectively. The beam velocity  $\beta = v_\infty/c$  is given in units of the velocity of

light  $c$  and  $m_0$  is the reduced mass of target and projectile. The Sommerfeld parameter  $\eta$  at a bombarding energy of 100 A MeV is illustrated in Fig. 1 as a function of the target charge number  $Z_2$  for various projectiles.

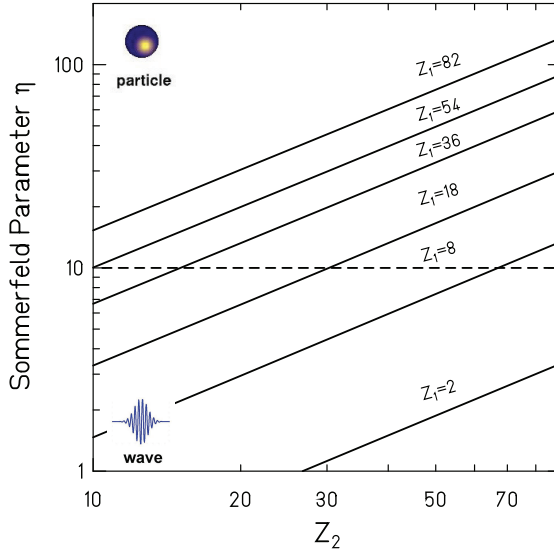


Fig. 1. Sommerfeld parameter  $\eta$  at a bombarding energy of 100 A MeV as a function of the target charge number  $Z_2$  for various projectiles. The boundary to quantum-mechanical corrections is determined at lower beam energies and indicated by the dashed line.

The condition  $\eta \gg 1$  ensures that one may form a wavepacket containing several waves and still having a size which is small compared to the dimensions of the classical trajectory. Such a wavepacket will move along a hyperbolic orbit exactly like a classical particle. For not too light projectile fragments scattered on a gold target  $\eta$  is still  $\gg 1$ , and the semi-classical description is appropriate.

In the semi-classical approach the projectile travels on well-defined orbits and the distance of closest approach  $D(\theta_{\text{cm}})$  or the impact parameter  $b(\theta_{\text{cm}})$  can be calculated from the measured scattering angle  $\theta_{\text{cm}}$

$$D(\theta_{\text{cm}}) = \frac{a}{\gamma} \times \left[ 1 + \sin^{-1} \left( \frac{\theta_{\text{cm}}}{2} \right) \right], \quad (2)$$

$$b(\theta_{\text{cm}}) = \frac{a}{\gamma} \times \text{ctg} \left( \frac{\theta_{\text{cm}}}{2} \right). \quad (3)$$

$\gamma = (1 - \beta^2)^{-1/2}$  is the relativistic Lorentz factor which is typically not much larger than one. From both expressions it is easy to calculate the following relation between the impact parameter  $b$  and the distance of closest approach  $D$

$$b = \sqrt{D^2 - \frac{2 \times a \times D}{\gamma}} \rightarrow D. \quad (4)$$

For large bombarding energies the impact parameter  $b$  becomes identical with the distance of closest approach  $D$ . Figure 2 illustrates the ratio  $b/R_{\text{int}}$  for a distance of closest approach  $D$  given by the nuclear interaction radius  $R_{\text{int}}$  as a function of the laboratory energy  $E_{\text{lab}}/A_1$ . For the system  $^{208}\text{Pb}+^{164}\text{Dy}$  Coulomb excitation at bombarding energies greater than 100 A MeV characterized by straight-line trajectories with impact parameters  $b$  larger than the sum of the radii of the colliding ions. For the present case the nuclear interaction radius is  $R_{\text{int}} = 15.5$  fm.

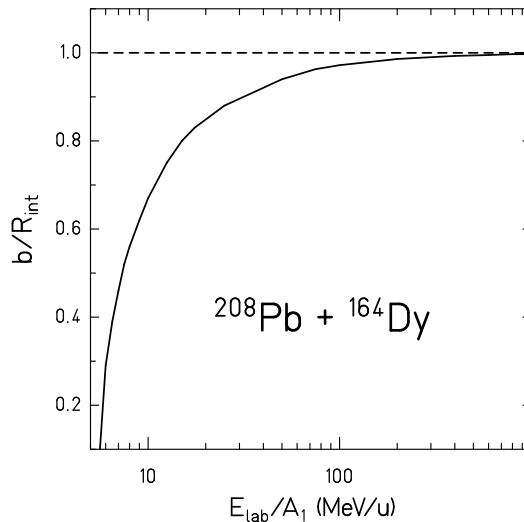


Fig. 2. Ratio of the impact parameter  $b$  and the nuclear interaction radius  $R_{\text{int}}$  versus the bombarding energy  $E_{\text{lab}}/A_1$  for the system  $^{208}\text{Pb}+^{164}\text{Dy}$ .

Another basic parameter in Coulomb excitation is the ratio of the collision time  $\tau_{\text{coll}}(\theta_{\text{cm}}) = \frac{a}{v_{\infty}} \sin^{-1}(\theta_{\text{cm}}/2)$  to the nuclear excitation time  $\tau_{\text{nucl}} = \hbar/\Delta E_{\text{exc}}$ , the so-called *adiabaticity parameter*  $\xi$

$$\xi(\theta_{\text{cm}}) = \frac{\Delta E_{\text{exc}}}{\hbar c} \times \frac{D(\theta_{\text{cm}})}{\beta\gamma}, \quad (5)$$

where  $\Delta E_{\text{exc}}$  is the excitation energy. For  $\xi \ll 1$  the process is sudden, and the excitation is possible; for  $\xi \gg 1$  the system follows adiabatically the time varying field and the excitation probability tends to zero. The value  $\xi = 1$  is the limit for the observation of Coulomb excitation and can be used for calculating the maximum energy transfer for a one step process. Figure 3 shows the maximum energy transfer for the system  $^{208}\text{Pb}+^{164}\text{Dy}$  as a function of the bombarding energy. In sub-barrier collisions the possible excitation energies are limited below 1–2 MeV. A possible way to overcome this limitation, and to excite high-lying states, is to use higher projectile energies.

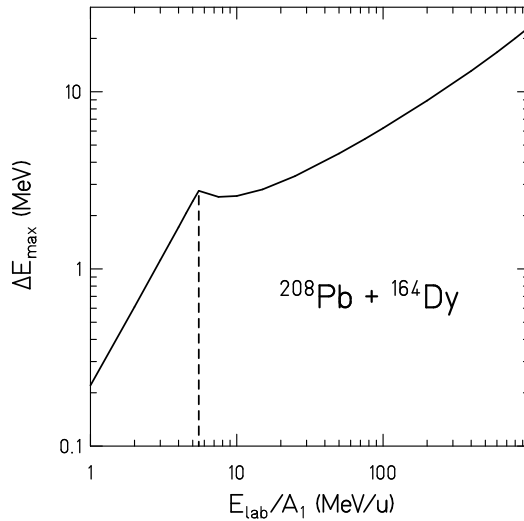


Fig. 3. Maximum energy transfer for single step excitation for Coulomb excitation of the system  $^{208}\text{Pb}+^{164}\text{Dy}$  as a function of the bombarding energy. The Coulomb barrier in the laboratory frame is indicated by the dashed line.

In the sudden approximation, one can treat the excitation of a rotational band and calculate the maximum angular momentum transfer by

$$\Delta L_{\text{max}} = \frac{3Z_1 e^2 Q_0}{8\hbar v_{\infty} a^2} \times J_{20}(\theta_{\text{cm}}) \quad (6)$$

with

$$J_{20}(\theta_{\text{cm}}) = \sin^2\left(\frac{\theta_{\text{cm}}}{2}\right) + \tan^2\left(\frac{\theta_{\text{cm}}}{2}\right) \times \left[1 - \frac{\pi - \theta_{\text{cm}}}{2} \times \tan\left(\frac{\theta_{\text{cm}}}{2}\right)\right], \quad (7)$$

where  $Q_0$  is the intrinsic quadrupole moment. For the system  $^{208}\text{Pb}+^{164}\text{Dy}$  with  $Q_0 = 7.5$  b the maximum angular momentum transfer is plotted in figure 4 as a function of the bombarding energy. One finds the largest angular momentum transfer for energies close to the Coulomb barrier.

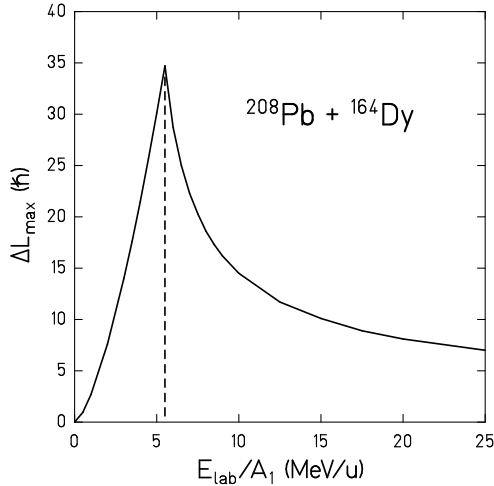


Fig. 4. Maximum angular momentum transfer for Coulomb excitation of the system  $^{208}\text{Pb}+^{164}\text{Dy}$  as a function of the bombarding energy. The Coulomb barrier in the laboratory frame is indicated by the dashed line.

In conclusion, single step excitation dominates for bombarding energies around and above 100 A MeV and states with energy up to 10–20 MeV can be readily excited.

#### 4. Conditions for Coulomb excitation

The basic assumption of a Coulomb excitation is that the charge distributions of projectile and target nucleus do not overlap at any time during the collision. At beam energies above the Coulomb barrier, the distance of closest approach, at which the nuclei still interact only electromagnetically, exceeds the sum of the nuclear radii by several fm. Figure 5 shows the measured inelastic cross-section divided by a theoretically calculated one *versus* the distance of closest approach for  $^{160}\text{Gd}+^{206,208}\text{Pb}$  [11] at energies close to the Coulomb barrier and for  $^{208}\text{Pb}+^{136}\text{Xe}$  [12] at 700 A MeV (Fig. 6). From both figures it is obvious, that at decreasing radial separation between the two ions, a drastic onset of the nuclear interaction with respect to the pure electromagnetic scattering occurs which is reflected in a drastic reduction of the inelastic cross-section. Moreover, since the data for the system  $^{160}\text{Gd}+^{206,208}\text{Pb}$  obtained for various bombarding energies as well as from two different projectiles seem to follow a common trend, it appears that the nuclear absorption basically depends on the distance of closest approach. From both experimental data-sets measured at low and high bombarding energies one can determine a ‘safe’ distance, at which a 1% deviation from

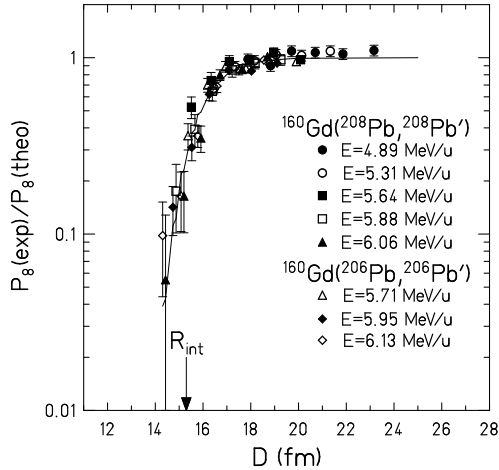


Fig. 5. Probability for populating the  $8^+$  level divided by a calculated probability *versus* the distance of closest approach  $D$  for the  $^{160}\text{Gd}+^{206,208}\text{Pb}$  systems at 8 different bombarding energies. The full line shows the results of a coupled channel calculation. The arrow marks the distance,  $D = R_{\text{int}}$ , for grazing collisions.

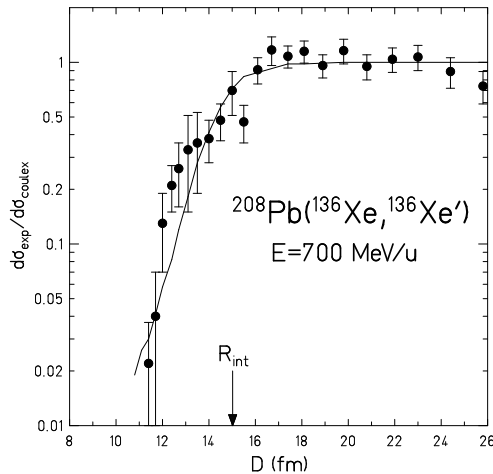


Fig. 6. Differential cross-section for the excitation of the one-phonon giant dipole resonance in  $^{136}\text{Xe}$  divided by a calculated cross-section *versus* the distance of closest approach  $D$  (Eq. 8) for the  $^{208}\text{Pb}+^{136}\text{Xe}$  system at 700 A MeV.

Coulomb excitation was observed. One needs a minimum distance between the two nuclear surfaces of at least 5 fm in order to assure pure electromagnetic interaction. The depicted curves represent an optical model calculation with the real and imaginary potential depths, the radius and the diffuseness parameters varied to fit the combined data.

For Coulomb trajectories in high-energy collisions, the extremely small scattering angles  $\vartheta_{\text{lab}}$  of the ion in the laboratory frame are related to  $D$  as

$$\vartheta_{\text{lab}} = \frac{2Z_1Z_2e^2}{m_1c^2\beta^2\gamma} \times \frac{1}{D} = \frac{2.88 \times Z_1Z_2 \times [931.5 + E_{\text{lab}}]}{A_1 \times [E_{\text{lab}}^2 + 1863 \times E_{\text{lab}}]} \times \frac{1}{D} \text{ [rad]}, \quad (8)$$

where  $E_{\text{lab}}$  is the laboratory beam energy in A MeV and  $m_1$  is the rest mass of the projectile. This approximation is valid for beam energies at  $\sim 100$  A MeV as shown in the appendix. In this way we can calculate the grazing angle  $\vartheta_{\text{gr}}(D = R_{\text{int}})$  for  $E_{\text{lab}} = 100$  A MeV which is the largest scattering angle in a Coulomb excitation experiment at relativistic energies. For all projectiles scattered on a  $^{197}\text{Au}$  target an angular range of about  $3^\circ$  (52 mrad) has to be covered by LYCCA-0.

## 5. Feasibility studies for future PreSPEC experiments

The experimental technique of relativistic Coulomb excitation was developed to take advantage of these higher beam energies and to obtain nuclear structure information even with low secondary-beam intensities but with very thick secondary targets. Typical RISING experiments were performed with projectile fragments of  $10^3$  ions/s on a gold target of  $0.4 \text{ g/cm}^2$  ( $\sim 10^{21}$  nuclei/cm $^2$ ). In the case of the  $2^+$  excitation in  $^{56}\text{Cr}$  the lowest inelastic cross-section of 90 mb was measured which yield an excitation probability of  $10^{-4}$ .

For the PreSPEC fast beam campaign with the higher photopeak efficiency of the AGATA demonstrator array, Coulomb excitation experiments on isomeric beams can also be performed. In fragmentation reactions angular momentum is transferred to the nuclei of interest (isomer-to-ground state ratio: 10–20%), which allows, after the separation in the fragment separator FRS, the investigation of higher-lying states beyond the yrast trap.

The following results were obtained with the program DWEIKO (Distorted Wave EIKOnal Approximation) [13] which calculates the elastic and inelastic scattering in nuclear collisions at intermediate and high energies. A coupled-channels method is used for Coulomb and nuclear excitations of  $E1$ ,  $E2$ ,  $E3$ ,  $M1$ , and  $M2$  multipolarities, respectively. Eikonal wave functions are used for the scattering, since both required conditions are valid at  $E_{\text{lab}} \geq 50$  A MeV: (a) forward scattering, *i.e.*  $\vartheta \ll 1$  radian, and (b) small energy transfer from the bombarding energy to the internal degrees of freedom of the projectile or target. For a given secondary beam and target, the probability of exciting a particular state  $I^\pi$  at a given energy  $\Delta E_{\text{exc}}$  in the projectile depends strongly on the incident beam energy. Figure 7 illustrates this dependence of the Coulomb excitation cross-section on the beam energy

for a  $^{136}\text{Xe}$  beam incident onto a secondary lead target. It shows the excitation of the first excited  $2^+$  and  $3^-$  states and the giant resonance states in Pb using the following reduced transition probabilities:  $B(E1) = 8$  W.u.,  $B(E2) = 9$  W.u. and  $B(E3) = 34$  W.u.. As one can see, beam energies below 100 A MeV are best suited for studying low-lying states, while energies above 300 A MeV are ideal for studying giant resonances. It is also apparent, that the quadrupole excitation to the  $2^+$  state at 4.086 MeV dominates over the octupole excitation to the  $3^-$  state at 2.614 MeV, which has a larger collective strength. For the excitation of the collective octupole state one obtains a cross-section of 29 mb which can be investigated with the new PreSPEC set-up.

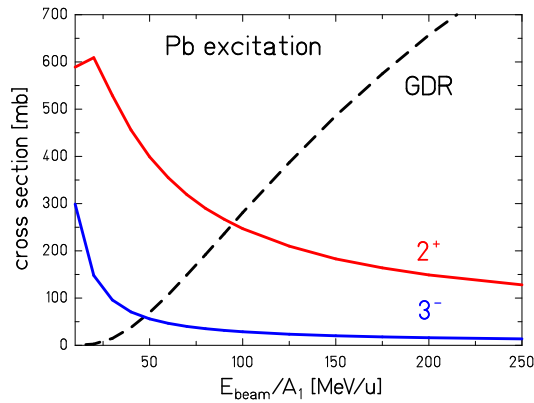


Fig. 7. Coulomb excitation cross-sections for the first excited  $2^+$  and  $3^-$  states and the giant dipole resonance (GDR) for a  $^{136}\text{Xe}$  beam incident on a lead target *versus* the beam energy. The calculation assumes a minimum impact parameter of 16 fm.

The cross-sections for magnetic excitation are very much smaller than for electric excitations at beam energies well below the Coulomb barrier; thus, even in cases where the  $\gamma$ -ray decay takes place by a mixed  $M1 + E2$  transition, the excitation will almost always be of rather pure  $E2$  type. Magnetic dipole excitations are reduced by a factor of  $(v/c)^2$  with respect to electric ones, apart from difference in nuclear matrix elements. Coulomb excitation experiments at relativistic energies are promising reactions to measure large  $M1$  transitions as shown in figure 8 for the system  $^{208}\text{Pb} + ^{85}\text{Br}$  with a strength of  $B(M1; 1/2^- \rightarrow 3/2^-) \sim 0.58\mu_N^2$ . Such a PreSPEC experiment can be performed with a  $^{85}\text{Br}$  beam of  $10^5$  ions/s, which requires new developments for the fragment identification before the secondary target.

The past decade has seen a rapid growth in the interest in properties of nuclei far from stability. Relativistic Coulomb excitation has been a very

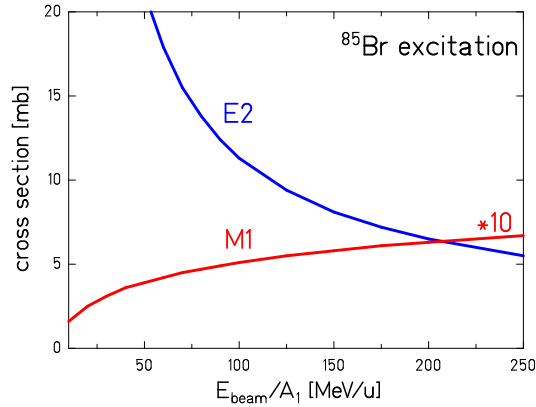


Fig. 8. Coulomb excitation cross-sections for  $M1$  and  $E2$  transitions for a  $^{85}\text{Br}$  beam incident on a lead target *versus* the beam energy. The calculation assumes a  $B(M1; 1/2^- \rightarrow 3/2^-) \sim 0.58\mu_N^2$ ,  $B(E2; 5/2^- \rightarrow 3/2^-) = 1.8$  W.u. and a minimum impact parameter of 14.2 fm.

successful tool to extract precious information on electromagnetic properties of nuclear transitions with relevance to nuclear structure as well as nuclear astrophysics. The new PreSPEC set-up with LYCCA-0 and the AGATA demonstrator array will improve the sensitivity of these measurements by more than an order of magnitude.

## Appendix

The scattering angle in the center of mass  $\theta_{\text{cm}}$  is related to the one in the laboratory  $\vartheta_{\text{lab}}$  by

$$\tan(\vartheta_{\text{lab}}) = \frac{\sin(\theta_{\text{cm}})}{\gamma_{\text{cm}} \times [\cos(\theta_{\text{cm}}) + \rho \times g(\rho, \epsilon_1)]}, \quad (9)$$

where,  $\rho = A_1/A_2$

$$\epsilon_1 = \frac{E_{\text{lab}}[A \text{ MeV}]}{m_N c^2}, \quad (10)$$

where  $m_N$  is the nucleon mass, and

$$g(\rho, \epsilon_1) = \frac{1 + \rho \times (1 + \epsilon_1)}{1 + \epsilon_1 + \rho}, \quad \gamma_{\text{cm}} = \frac{1 + \epsilon_1 + \rho}{\sqrt{(1 + \rho)^2 + 2\rho\epsilon_1}}, \quad (11)$$

$\gamma_{\text{cm}}$  is the relativistic Lorentz factor of the motion of the center of mass system with respect to the laboratory. For the system  $^{208}\text{Pb} + ^{136}\text{Xe}$  with

a nuclear interaction radius of  $D = R_{\text{int}} = 15.1$  fm ( $\theta_{\text{cm}}$  given by Eq. (2)) the scattering angle in the laboratory is calculated for a beam energy of 100 A MeV and 700 A MeV and compared in the table below with the results of the approximation (Eq. (8)).

TABLE I

$^{208}\text{Pb} + ^{136}\text{Xe}; D = R_{\text{int}} = 15.1$ fm	$\vartheta_{\text{lab}}$ (exact, Eq. (9))	$\vartheta_{\text{lab}}$ (approx., Eq. (8))
$E_{\text{lab}} = 100$ A MeV	1.862°	1.866°
$E_{\text{lab}} = 700$ A MeV	0.272°	0.323°

## REFERENCES

- [1] H.J. Wollersheim *et al.*, *Nucl. Instrum. Methods* **A537**, 637 (2005).
- [2] R. Lozeva *et al.*, *Nucl. Instrum. Methods* **A562**, 298 (2006).
- [3] A. Bürger *et al.*, *Phys. Lett.* **B622**, 29 (2005).
- [4] A. Banu *et al.*, *Phys. Rev.* **C72**, 061305 (2005).
- [5] T.R. Saito *et al.*, *Phys. Lett.* **B669**, 19 (2008).
- [6] O. Wieland *et al.*, *Phys. Rev. Lett.* **102**, 092502 (2008).
- [7] HISPEC: High-Resolution In-Flight SPECTroscopy; DISPEC: DEcay SPECTroscopy, Technical Proposal, [www.gsi.de/fair/experiments/NUSTAR/Proposals.html](http://www.gsi.de/fair/experiments/NUSTAR/Proposals.html)
- [8] NuSTAR: NUClear STructure, Astrophysics and Reactions, [www.gsi.de/nustar](http://www.gsi.de/nustar); R. Krücken, *J. Phys. G* **204**, 71 (2003).
- [9] Facility for Antiproton and Ion Research, [www.gsi.de/fair](http://www.gsi.de/fair)
- [10] AGATA: Advanced GAMMA Tracking Array, Technical Proposal, in J. Gerl, W. Korten (Ed.) GSI Darmstadt, 2001; J. Simpson, *J. Phys. G* **31**, S1801 (2005).
- [11] F.W.N. de Boer *et al.*, *Z. Phys.* **A325**, 457 (1986).
- [12] A. Grünschloss *et al.*, *Phys. Rev.* **C60**, 051601 (1999).
- [13] C.A. Bertulani *et al.*, *Comput. Phys. Commun.* **152**, 317 (2003).